Dark noise and retinal degeneration from D190N-rhodopsin

Daniel Silverman[a,b,1,2], Zuying Chai[a,1], Wendy W. S. Yue[a,3], Sravani Keerthi Ramisetty[c], Sowmya Bekshe Lokappa[c], Kazumi Sakai[d], Rikard Frederiksen[e], Parinaz Bina[a,4], Stephen H. Tsang[f,g], Takahiro Yamashita[d], Jeannie Chen[c], and King-Wai Yau[a,h,5]

[a]Solomon H. Snyder Department of Neuroscience, Johns Hopkins University School of Medicine, Baltimore, MD 21205; [b]Biochemistry, Cellular and Molecular Biology Graduate Program, Johns Hopkins University School of Medicine, Baltimore, MD 21205; [c]Zilkha Neurogenetic Institute, Department of Physiology and Biophysics, Keck School of Medicine, University of Southern California, Los Angeles, CA 90089; [d]Department of Biophysics, Graduate School of Science, Kyoto University, Kyoto 606-8502, Japan; [e]Jules Stein Eye Institute, University of California, Los Angeles, CA 90095; [f]Department of Ophthalmology, Columbia Stem Cell Initiative, Columbia University, New York, NY 10032; [g]Department of Pathology and Cell Biology, Columbia Stem Cell Initiative, Columbia University, New York, NY 10032; and [h]Department of Ophthalmology, Johns Hopkins University School of Medicine, Baltimore, MD 21205

Contributed by King-Wai Yau, July 31, 2020 (sent for review May 27, 2020; reviewed by Ching-Kang Jason Chen and Daniel D. Oprian)

Numerous rhodopsin mutations have been implicated in night blindness and retinal degeneration, often with unclear etiology. D190N-rhodopsin (D190N-Rho) is a well-known inherited human mutation causing retinitis pigmentosa. Both higher-than-normal spontaneous-isomerization activity and misfolding/mistargeting of the mutant protein have been proposed as causes of the disease, but neither explanation has been thoroughly examined. We replaced wild-type rhodopsin (WT-Rho) in *Rho*$^{D190N/WT}$ mouse rods with a largely "functionally silenced" rhodopsin mutant to isolate electrical responses triggered by D190N-Rho activity, and found that D190N-Rho at the single-molecule level indeed isomerizes more frequently than WT-Rho by over an order of magnitude. Importantly, however, this higher molecular dark activity does not translate into an overall higher cellular dark noise, owing to diminished D190N-Rho content in the rod outer segment. Separately, we found that much of the degeneration and shortened outer-segment length of *Rho*$^{D190N/WT}$ mouse rods was not averted by ablating rod transducin in phototransduction—also consistent with D190N-Rho's higher isomerization activity not being the primary cause of disease. Instead, the low pigment content, shortened outer-segment length, and a moderate unfolded protein response implicate protein misfolding as the major pathogenic problem. Finally, D190N-Rho also provided some insight into the mechanism of spontaneous pigment excitation.

D190N-rhodopsin | spontaneous isomerization | protein misfolding | night blindness | retinitis pigmentosa

Our dark-adapted visual system has an exceedingly low threshold for perceiving light (1), imparted largely by rhodopsin in several ways, namely, the high density of rhodopsin packed into each rod to ensure a high photon-capture ability (2), rhodopsin's substantial signal amplification to provide a sizeable single-photon response (3–5), and rhodopsin's low spontaneous excitation to minimize false signaling, or dark noise (6, 7). As the most abundant protein in rods, rhodopsin also supports the structure of the outer segment, sustaining photoreceptor health and survival (8–11). Various forms of night blindness and retinal degeneration have been linked to single-amino acid substitutions in rhodopsin (12). For example, G90D-Rho has been found to elevate spontaneous activity to such an extent as to produce rod desensitization similar to light adaptation (13–15). Other familial rhodopsin mutations have been similarly speculated to elevate dark noise to produce desensitization or even cell damage (16–19). Certain mutations may cause deficits in signal amplification (20), and still others could lead to protein misfolding/mistargeting, ultimately resulting in cell death and vision loss (21–24). Much of what is known about rhodopsin mutants has come from in vitro studies of heterologously expressed mutants (25–30). Thus, with only a few animal models generated, the exact deleterious effects of many rhodopsin mutations in rods remain obscure or unsolved.

D190N-rhodopsin (D190N-Rho) is a well-known mutation and exemplifies a case of longstanding mechanistic uncertainty, in that past studies have led to a debate over this mutant pigment's reduced ability to fold properly (26, 27) versus the possibility of higher-than-normal dark noise in a live mammalian rod (16, 19, 31, 32), or both. This mutation was found in several families with autosomal-dominant retinitis pigmentosa (26, 27, 33, 34), with heterozygous (*Rho*$^{D190N/WT}$) patients first reporting poor night vision early in life (33) and subsequently showing retinal degeneration (by age ~50, for example) (32–34). The pathology for

Significance

Rhodopsin mutations account for ~30% of autosomal-dominant retinitis pigmentosa cases. While dozens of distinct mutations have been identified, the reported detriments that they cause in cell culture are not necessarily all consistent across studies and have often not been evaluated in animal models. Even when an animal model is available, it is typically not straightforward to isolate mutant-rhodopsin signals from related endogenous-rhodopsin signals. Here, we introduce an approach employing a largely "functionally silenced" endogenous rhodopsin in rods as background for isolating activity due to D190N-rhodopsin (D190N-Rho). We conclude that, despite D190N-Rho's elevated molecular rate constant of spontaneous activation, it does not increase the overall cellular dark noise of the rod, thus excluding its increased noise as the reason for disease.

Author contributions: D.S., Z.C., W.W.S.Y., J.C., and K.-W.Y. designed research; D.S., Z.C., W.W.S.Y., S.K.R., S.B.L., K.S., R.F., P.B., and J.C. performed research; S.H.T. contributed new reagents/analytic tools; D.S., Z.C., P.B., T.Y., J.C., and K.-W.Y. analyzed data; and D.S., Z.C., W.W.S.Y., J.C., and K.-W.Y. wrote the paper.

Reviewers: C.-K.J.C., Baylor College of Medicine; and D.D.O., Brandeis University.

The authors declare no competing interest.

[1]D.S. and Z.C. contributed equally to this work.

[2]Present address: Division of Neurobiology, Department of Molecular and Cell Biology, Helen Wills Neuroscience Institute, Howard Hughes Medical Institute, University of California, Berkeley, CA 94720.

[3]Present address: Department of Physiology, University of California, San Francisco, CA 94158.

[4]Present address: Department of Animal and Avian Sciences, University of Maryland, College Park, MD 20742.

[5]To whom correspondence may be addressed. Email: kyau1@jhmi.edu.

This article contains supporting information online at https://www.pnas.org/lookup/suppl/doi:10.1073/pnas.2010417117/-/DCSupplemental.

First published September 1, 2020.

homozygous ($Rho^{D190N/D190N}$) patients is unknown because they have not been reported in clinical studies. Broader interest in D190N-Rho came from the high conservation of rhodopsin's native D190 amino acid residue across rod and cone pigments and from its intriguing structural position in the protein—forming, together with another highly conserved residue (R177), a salt bridge directly above the chromophore-binding pocket (31). Biochemical experiments suggested that disruption of this salt bridge in D190N-Rho destabilized dark-state rhodopsin to give the mutant pigment a spontaneous isomerization rate higher than normal (16, 31, 35). However, these in vitro observations may not provide direct information about the situation in vivo.

Recently, a D190N-Rho knockin mouse was generated (32), but it did not readily allow isolation of D190N-Rho activity from endogenous wild-type (WT)-Rho activity in $Rho^{D190N/WT}$ heterozygous animals. At the same time, $Rho^{D190N/D190N}$ homozygous rods degenerate very rapidly (19), making recordings infeasible already at eye opening. To largely silence endogenous WT-Rho activity while maintaining outer-segment structure for recording, we bred $Rho^{D190N/D190N}$ with $Rho^{REY/REY}$ mice (3) to obtain $Rho^{D190N/REY}$ mice so as to replace WT-Rho with REY-Rho. In REY-Rho, the amino acid sequence ERY in the G-protein (transducin)–binding motif has been changed to REY, causing no apparent change in light absorption, only a small change in pigment-protein expression, but a huge reduction (by many thousands of times) in the coupling efficiency between pigment and transducin, rendering the pigment largely "functionally silenced" (3, 20). This genotype allows us to isolate D190N-Rho's single-photon response, and to also quantify its content as well as its dark spontaneous activity in $Rho^{D190N/REY}$ rods. At the same time, such measurements provide an opportunity for us to check D190N-Rho's activity against our recently developed physicochemical theory of spontaneous pigment isomerization (7). Finally, the general strategy described here may be useful for elucidating the disease mechanisms of some other rhodopsin mutations implicated in night blindness and retinal degeneration.

Results

$Rho^{D190N/WT}$ Mouse Rods Had Lower Flash Sensitivity and Faster Response Kinetics than $Rho^{WT/WT}$ Rods. Because the D190N mutation typically occurs in the heterozygous state in patients, we started by measuring flash responses from single $Rho^{D190N/WT}$ mouse rods (referred to as $Rho^{D190N/+}$ in ref. 32). Compared to $Rho^{WT/WT}$ (C57BL/6J) rods (Fig. 1*A*, black), $Rho^{D190N/WT}$ rods showed flash responses with faster kinetics (Fig. 1*A*, green), a smaller saturated-response amplitude (Fig. 1*A* and *SI Appendix*, Table S1A), and ~5.5-fold lower sensitivity based on the shift in intensity–response relation along the flash intensity axis (Fig. 1*B*). These effects were broadly in line with previous electroretinographic data from $Rho^{D190N/WT}$ mice and humans (32–34). The comparison between the normalized, averaged dim-flash responses from $Rho^{WT/WT}$ and from $Rho^{D190N/WT}$ rods is given in Fig. 1*C*, showing the latter's faster response decay. One cannot, however, isolate the behavior of the D190N-Rho single-photon response from that of WT-Rho in $Rho^{D190N/WT}$ rods because the fluctuation analysis for extracting the single-photon response requires a homogeneous population of pigment molecules, which is not the case here.

Isolation of the D190N-Rho Response. To isolate D190N-Rho responses without removing WT-Rho, which otherwise would compromise the structural support provided by rhodopsin in the outer segment (9), we instead silenced WT-Rho signaling (although not fully) by replacing it with a mutant rhodopsin, REY-Rho, which has a disrupted G-protein–binding site (3, 20) (see Introduction]. In $Rho^{REY/REY}$ mouse rods, REY-Rho is expressed at near-normal levels (3), which helps to maintain outer-segment structure for recordings. The 500-nm light absorption by detergent-solubilized whole $Rho^{REY/REY}$ retinae likewise demonstrated that the REY-Rho content, at 0.31 ± 0.02 nmol per retina (n = 4 retinae), was similar to that for $Rho^{WT/WT}$ mice (9). There is no change in protein level of any phototransduction signaling component (3). However, $Rho^{REY/REY}$ rods were ~16,000-fold less sensitive than $Rho^{WT/WT}$ rods (Fig. 1 *A* and *B*). The reason for such low sensitivity is that REY-Rho, upon absorbing a photon, triggers phototransduction with such an exceedingly low probability of success that, even when successful, no more than a single downstream transducin/phosphodiesterase effector complex is activated, giving a relatively tiny electrical response (3). As such, we found no clearly detectable responses from $Rho^{REY/REY}$ rods at flash strengths up to ~10,000 photons·μm^{-2} (Fig. 1*A*, gray; see legend), although, at high enough intensities, the rarely successful and tiny single-REY-Rho–triggered events still summed to give measurable macroscopic responses (Fig. 1*B*, gray). At a flash intensity of ~30 photons·μm^{-2}, the light responses elicited from $Rho^{D190N/REY}$ rods were composed practically entirely of photosignals from D190N-Rho (Fig. 1 *A* and *B*, red). $Rho^{WT/REY}$ rods, in comparison, showed a higher sensitivity than $Rho^{D190N/REY}$ rods (Fig. 1*B*, blue). Fluctuation analysis of a response ensemble elicited from $Rho^{D190N/REY}$ rods by repeated, identical dim flashes demonstrated that D190N-Rho's single-photon response was actually fairly similar to that for WT-Rho in $Rho^{WT/WT}$ rods (Fig. 1*D*). Both responses had very similar rising phases and times-to-peak (t_{peak}) (Fig. 1*D*), but D190N-Rho responses decayed ~40% faster, with a shorter recovery time constant (τ_{Rec}) and a shorter integration time (t_{int}) (Fig. 1 *D* and *E*).

One possible reason for the faster response decline in $Rho^{D190N/REY}$ rods was the alleged higher dark spontaneous activity of D190N-Rho compared to WT-Rho, acting as an "equivalent background light" to trigger adaptation as does real background light (see Introduction). The puzzle, however, is that such an adaptation to background light is typically accompanied by a reduction in the single-photon response amplitude (36, 37), which was surprisingly insignificant here (Fig. 1*D* and *SI Appendix*, Table S1A). Interestingly, WT-Rho's single-photon response in heterozygous rhodopsin-knockout $Rho^{WT/-}$ rods [commonly referred to as $Rho^{+/-}$ (9)] happens to also have a faster response decline and an unaffected peak amplitude (10, 38). Such a resemblance in single-photon response kinetics between $Rho^{WT/-}$ and $Rho^{D190N/REY}$ suggests that they may have a common cause, namely, a lower pigment content in the rods. $Rho^{WT/-}$ rods have ~50% of the rhodopsin content in $Rho^{WT/WT}$ (9). Associated with this lower rhodopsin content is a ~30% shorter outer segment and a smaller interdiskal space in $Rho^{WT/-}$ rods, which have been proposed to result in a faster response decline by accelerating Ca^{2+}-mediated negative feedback (10, 11). Similarly, the outer-segment length of $Rho^{WT/REY}$ rods was ~11% shorter, and also accompanied by a faster response decay (Fig. 1*D*, blue; *SI Appendix*, Table S1A). We found even shorter outer-segment lengths in the $Rho^{D190N/REY}$ and $Rho^{D190N/WT}$ rods that we recorded from, both being ~40% shorter than in $Rho^{WT/WT}$ rods (*SI Appendix*, Table S1A). All in all, the overall rhodopsin content in $Rho^{D190N/REY}$ and $Rho^{D190N/WT}$ rods may indeed be lower than normal.

Measurement of D190N-Rho Content in $Rho^{D190N/REY}$ Rods. To quantify D190N-Rho content in $Rho^{D190N/REY}$ rods, we bred these mice into the $Gcaps^{-/-}$ background to give the $Rho^{D190N/REY}$;$Gcaps^{-/-}$ genotype, which facilitates the measurement of D190N-Rho's single-photon responses by increasing their amplitude to approximately fivefold as large through removing a major Ca^{2+}-mediated negative feedback (39–41). Incidentally, we found that removing this feedback mechanism resulted in $Rho^{D190N/REY}$;$Gcaps^{-/-}$ rods having similar, instead of faster, single-photon response kinetics compared to $Rho^{WT/WT}$;$Gcaps^{-/-}$ rods (Fig. 2*B* and *SI Appendix*, Table S1B; see also Fig. 3*B*). This observation may fit with the

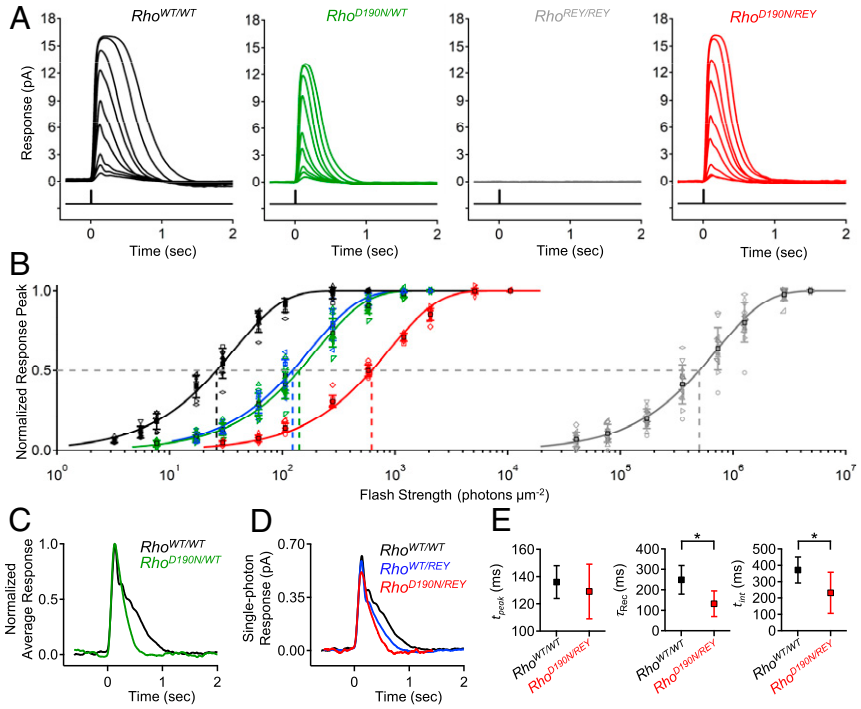

Fig. 1. Lower flash sensitivity and faster response kinetics of $Rho^{D190N/WT}$ rods compared to WT, and isolation of D190N-Rho responses in $Rho^{D190N/REY}$. (*A*) Flash response families for $Rho^{WT/WT}$ (C57BL/6J, black), $Rho^{D190N/WT}$ (green), $Rho^{REY/REY}$ (gray), and $Rho^{D190N/REY}$ (red) rods. REY-Rho responses were not observed in $Rho^{REY/REY}$ rods in a flash response family of ~30 to 10,000 photons·μm^{-2}·s^{-1}, while D190N-Rho responses were robust in $Rho^{D190N/REY}$ rods over the same range. (*B*) Intensity–response relations of normalized response peak versus flash strength for each genotype shown in *A* in addition to that of $Rho^{WT/REY}$ rods. The solid curves are fits to a saturating-exponential function (*Methods*) with half-saturating flash strengths (ρ) of 26 ($Rho^{WT/WT}$), 142 ($Rho^{D190N/WT}$), 124 ($Rho^{WT/REY}$), 622 ($Rho^{D190N/REY}$), and 502,754 ($Rho^{REY/REY}$) photons·μm^{-2}. (*C*) Normalized, averaged dim-flash responses for $Rho^{WT/WT}$ rods (black) and $Rho^{D190N/WT}$ rods (green). (*D*) Single-photon responses (obtained from quantal fluctuation analysis) of WT-Rho in $Rho^{WT/WT}$ rods (black), D190N-Rho in $Rho^{D190N/REY}$ rods (red), and WT-Rho in $Rho^{WT/REY}$ (blue). (*E*, *Left*) Time-to-peak (t_{peak}) of single-photon responses from WT-Rho (black) and D190N-Rho (red); t_{peak} = 136 ± 12 ms ($Rho^{WT/WT}$; n = 9 cells) and 129 ± 20 ms ($Rho^{D190N/REY}$; n = 12 cells). (*E*, *Center*) Recovery time constant (τ_{Rec}) from fitting the final exponential decline of the single-photon response; τ_{Rec} = 249 ± 70 ms ($Rho^{WT/WT}$), 132 ± 63 ms ($Rho^{D190N/REY}$). (*E*, *Right*) Integration time (t_{int}) of single-photon response (defined as the time integral of single-photon response divided by transient peak amplitude), t_{int} = 371 ± 79 ms ($Rho^{WT/WT}$), 232 ± 126 ms ($Rho^{D190N/REY}$). The single stars mark statistical significance of 0.0001 ≤ P ≤ 0.05 from Student's t tests. There was no statistically significant difference in time-to-peak.

proposal mentioned earlier that Ca^{2+}-mediated negative feedback underlies the faster response decline in $Rho^{D190N/REY}$ rods (see Fig. 1*D*).

To estimate the D190N-Rho content in $Rho^{D190N/REY}$ rods, we delivered repeated, identical dim flashes to a rod (Fig. 2*A*) and measured the probability of failure (i.e., the fraction of flash trials that elicited no detectable responses). Based on the Poisson distribution of photon absorption (42) (*Methods*), this probability of failure readily gives an estimate of the number of rhodopsin molecules capable of triggering normal-sized single-photon responses (i.e., excluding REY-Rho and also mistargeted/misfolded, thus nonfunctional, D190N-Rho). As such, we obtained (4.8 ± 1.3) × 10^6 functional D190N-Rho molecules in a $Rho^{D190N/REY}$;$Gcaps^{-/-}$ rod (Fig. 2*C*, red; n = 12 rods). The same flash strength did not elicit noticeable responses in $Rho^{REY/REY}$;$Gcaps^{-/-}$ rods owing to REY-Rho's extremely poor efficiency to interact with transducin and to its small associated single-photon responses (Fig. 2*A*, gray). The same probability-of-failure experiment on $Rho^{WT/WT}$;$Gcaps^{-/-}$ rods gave (8.8 ± 3.4) × 10^7 Rho molecules in a WT rod (Fig. 2*C*, black; n = 23 rods). Thus, the functional D190N-Rho content in $Rho^{D190N/REY}$;$Gcaps^{-/-}$ was only 5.5% of the WT-Rho content in $Rho^{WT/WT}$;$Gcaps^{-/-}$ rods (Fig. 2*C*). The low pigment content in $Rho^{D190N/REY}$;$Gcaps^{-/-}$ rods was confirmed independently by microspectrophotometry (Fig. 2*D*), and in $Rho^{D190N/REY}$ rods by physiological action spectra as well as biochemical isoelectric-focusing experiments (*SI Appendix, Supplementary Text* and Fig. S1).

To check whether any of the diminished functional D190N-Rho pigment content was simply due to a weaker binding of chromophore to D190N-apo-opsin, thus reducing holopigment formation, we exposed dark-adapted $Rho^{D190N/REY}$ rods to excess chromophore (50 μM 11-*cis*-retinal for 15 min), but found no increase in holo-pigment content as evaluated by microspectrophotometry (Fig. 2*D*). There was also no sign of extra apo-opsin noise (3) in dark-adapted $Rho^{D190N/REY}$;$Gcaps^{-/-}$ rods; their steady noise variance (0.14 ± 0.08 pA^2, n = 5 rods) was similar to that in $Rho^{WT/WT}$;$Gcaps^{-/-}$ rods (0.17 ± 0.11 pA^2; n = 17).

Molecular Spontaneous Activity of D190N-Rho Measured in $Rho^{D190N/REY}$ Rods. As pointed out earlier, $Rho^{D190/REY}$ rods offer the opportunity to isolate D190N-Rho activity from WT-Rho activity. Fig. 2 *E*–*G* show dark recordings from $Rho^{WT/WT}$;$Gcaps^{-/-}$, $Rho^{REY/REY}$;$Gcaps^{-/-}$, and $Rho^{D190/REY}$;$Gcaps^{-/-}$ rods. $Rho^{WT/WT}$;$Gcaps^{-/-}$ rods exhibited occasional dark events (marked by stars) resembling normal-sized single-photon responses. From collected data, we obtained an average cellular spontaneous-isomerization rate at 37 °C of 0.008 ± 0.004 s^{-1}·cell^{-1} (n = 17 rods; Fig. 2*H*, black), similar to past measurements (7, 39–41). There were no prominent dark events in $Rho^{REY/REY}$;$Gcaps^{-/-}$ rods, as expected. $Rho^{D190/REY}$;$Gcaps^{-/-}$ rods showed similar dark events as $Rho^{WT/WT}$;$Gcaps^{-/-}$ rods, with collected data giving 0.007 ± 0.003 s^{-1}·cell^{-1} (n = 12 rods; Fig. 2*H*, red). Dividing the average cellular isomerization rates in $Rho^{WT/WT}$;$Gcaps^{-/-}$ rods and $Rho^{D190/REY}$;$Gcaps^{-/-}$ rods by their respective functional

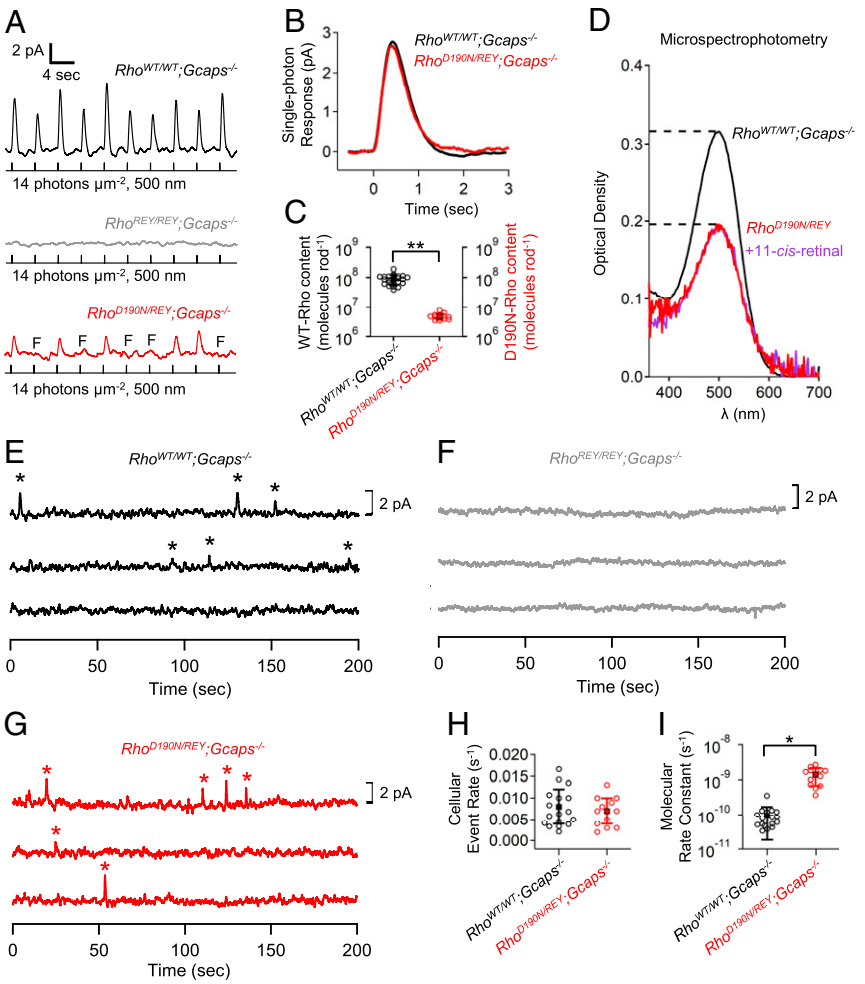

Fig. 2. Pigment content and spontaneous activity of $Rho^{D190N/REY}$ rods. (*A*) Repeated dim flashes at the same flash strength (14 photons·µm^{-2}) on $Rho^{WT/WT}$;$Gcaps^{-/-}$ rods (black) reliably triggered responses, while $Rho^{REY/REY}$;$Gcaps^{-/-}$ rods (gray) did not show any discernible responses because of severely weakened interaction between REY-Rho and G protein. $Rho^{D190N/REY}$;$Gcaps^{-/-}$ rods (red) exhibited a higher probability of failure (red, response failures marked by "F") compared to $Rho^{WT/WT}$;$Gcaps^{-/-}$. (*B*) Single-photon responses from WT-Rho in $Rho^{WT/WT}$;$Gcaps^{-/-}$ and D190N-Rho in $Rho^{D190N/REY}$;$Gcaps^{-/-}$ rods. Waveforms are ensemble averages from all cells of each genotype. (*C*) Functional rhodopsin content in each genotype based on the measured probability of failure (*Methods*). The double stars mark statistical significance of $P < 0.0001$. (*D*) Microspectrophotometry measuring optical density in a group of outer segments extending from a piece of retina. Peak optical density was 0.316 ± 0.087 in $Rho^{WT/WT}$;$Gcaps^{-/-}$. Data were reproduced from ref. 3 because the corresponding measurements were not made with $Rho^{WT/WT}$;$Gcaps^{+/+}$ rods. There is no reported difference in WT-Rho content between the $Gcaps^{-/-}$ and $Gcaps^{+/+}$ backgrounds. Peak optical density was 0.187 ± 0.037 in $Rho^{D190N/REY}$;$Gcaps^{+/+}$ (red; $n = 4$ retinal regions, 2 animals). To assess any excess apo-opsin content in $Rho^{D190N/REY}$, rods were exposed to excess 11-*cis*-retinal (50 µM for 15 min; *SI Appendix, Supplementary Methods*) and optical density was measured again (purple). Peak optical density did not significantly increase after retinal exposure, 0.196 ± 0.028 ($n = 4$ retinal regions, 2 animals; $P = 0.62$, Student's *t* test). (*E* and *F*) WT-Rho produced discrete dark-noise events (indicated with stars) in $Rho^{WT/WT}$;$Gcaps^{-/-}$ rods, which were functionally silenced by replacing WT-Rho with REY-Rho in $Rho^{REY/REY}$;$Gcaps^{-/-}$ rods. (*G*) Discrete noise events from D190N-Rho could be clearly identified to determine their frequency in $Rho^{D190N/REY}$;$Gcaps^{-/-}$ rods. (*H*) Cellular rate of spontaneous-isomerization events in $Rho^{WT/WT}$;$Gcaps^{-/-}$ and $Rho^{D190N/REY}$;$Gcaps^{-/-}$. (*I*) Molecular rate constant of spontaneous isomerization for WT-Rho in $Rho^{WT/WT}$;$Gcaps^{-/-}$ and for D190N-Rho in $Rho^{D190N/REY}$;$Gcaps^{-/-}$ rods. The single star marks statistical significance of $0.0001 \le P \le 0.05$.

pigment content described in the previous section, we obtained the molecular spontaneous activities at 37 °C, being ~9.1×10^{-11} s^{-1} for WT-Rho and ~1.5×10^{-9} s^{-1} for D190N-Rho (Fig. 2*I*). Hence, D190N-Rho's spontaneous molecular isomerization rate is 16-fold as high as WT-Rho's. However, the resulting dark noise at the cellular level is practically unchanged, owing to the low D190N-Rho content in $Rho^{D190N/REY}$ rods. Incidentally, the molecular spontaneous activity of WT-Rho appeared to be similar in $Rho^{WT/REY}$;$Gcaps^{-/-}$ and in $Rho^{WT/WT}$;$Gcaps^{-/-}$ rods, as one might expect (*SI Appendix*, Fig. S2*F*).

***Rho*$^{D190N/WT}$ Genotype.** With the $Rho^{D190/REY}$ genotype, it is straightforward to quantify D190N-Rho's molecular spontaneous activity with electrophysiology. However, because the $Rho^{D190N/WT}$ genotype is exactly what corresponds to that of human patients, we repeated the same measurements on this genotype with the additional help of biochemistry to estimate D190N-Rho content. From the probability-of-failure experiment with identical dim flashes (Fig. 3*A*), we estimated the total functional pigment content (i.e., D190N-Rho and WT-Rho together) in $Rho^{D190N/WT}$;$Gcaps^{-/-}$ rods to be $(3.2 \pm 1.6) \times 10^7$ molecules·rod^{-1} (Fig. 3*D*, green; $n = 16$ rods), also lower than in $Rho^{WT/WT}$;$Gcaps^{-/-}$ rods (Fig. 3*D*, black). Next, from dark-noise measurements (Fig. 3*C*), the cellular rate of spontaneous events of $Rho^{D190N/WT}$;$Gcaps^{-/-}$ rods was 0.009 ± 0.005 s^{-1} (Fig. 3*E*, green; $n = 16$ rods), also similar to that of $Rho^{WT/WT}$;$Gcaps^{-/-}$ rods—perhaps not surprising, given the

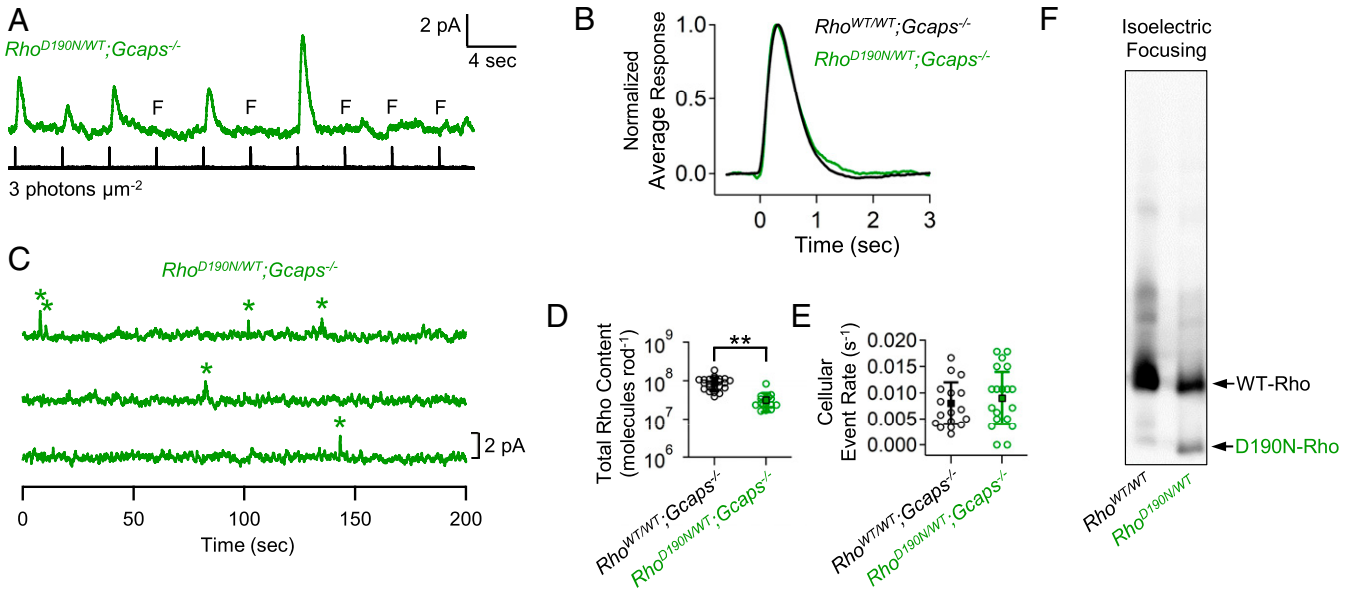

Fig. 3. Pigment content and spontaneous activity of $Rho^{D190N/WT}$ rods. (*A*) Series of dim-flash responses from $Rho^{D190N/WT}$;$Gcaps^{-/-}$ (green) rods. (*B*) Normalized ensemble averages of dim-flash responses from $Rho^{WT/WT}$;$Gcaps^{-/-}$ and $Rho^{D190N/WT}$;$Gcaps^{-/-}$ rods (n = 23 and 16 rods, respectively). (*C*) Dark noise from a $Rho^{D190N/WT}$;$Gcaps^{-/-}$ rod with discrete events marked by stars. (*D*) Functional pigment content estimated from the probability of failure (*Methods*) in $Rho^{WT/WT}$;$Gcaps^{-/-}$ (same as in Fig. 2*C*) and $Rho^{D190N/WT}$;$Gcaps^{-/-}$ rods. Double stars mark statistical significance of $P < 0.0001$. (*E*) Cellular rate of spontaneous isomerization events. Each open symbol represents the estimate from an individual rod. There was not a significant difference in cellular event rate between these genotypes. (*F*) Isoelectric focusing blot showing distinct D190N-Rho (~35% of total pigment) and WT-Rho (~65% of total pigment) bands.

findings from $Rho^{D190/REY}$;$Gcaps^{-/-}$ rods in the previous section. The similar kinetics in the dim-flash responses between $Rho^{WT/WT}$;$Gcaps^{-/-}$ and $Rho^{D190N/WT}$;$Gcaps^{-/-}$ rods have been commented before in connection with Fig. 2*B*.

To estimate the content ratio of D190N-Rho to WT-Rho molecules in $Rho^{D190N/WT}$ rods, we employed the biochemical method of isoelectric focusing (43, 44), which separated the two rhodopsin molecular species according to their distinct isoelectric points. In this genotype, we found the pigment content to consist of 35 ± 4% D190N-Rho and 65 ± 4% WT-Rho (Fig. 3*F*; n = 5 retinae), or a ratio of roughly one D190N-Rho for every two WT-Rho molecules.

Using the spontaneous molecular rate constant of 9.1×10^{-11} s^{-1} for WT-Rho from the previous section, we obtained, after some calculations from the above measurements, a molecular rate constant of 6.3×10^{-10} s^{-1} for D190N-Rho, about a factor of 2 less than that obtained from $Rho^{D190/REY}$;$Gcaps^{-/-}$ rods described above. Considering the rather round-about way of making calculations from the above $Rho^{D190N/WT}$ rod measurements, such a discrepancy is not major.

In summary, in the $Rho^{D190N/WT}$ disease genotype, as in the $Rho^{D190/REY}$ genotype, D190N-Rho's content is likewise low enough that, despite its much higher molecular isomerization rate than WT-Rho, the cellular isomerization rate is no greater than normal.

D190N-Rho's Elevated Spontaneous Activity Is Not High Enough to Trigger Adaptation. With so much past speculation about D190N-Rho and other noisy rhodopsin mutants (16, 19, 45) causing "equivalent-light adaptation," we were curious about how high rhodopsin's spontaneous-isomerization rate would have to be in order to desensitize mouse rods substantially. Fig. 4*A* shows the effect of steady background light on flash sensitivity in $Rho^{WT/WT}$ (C57BL/6J) rods. Dim-flash sensitivity was reduced to ~50% by a background light of 57 photons·μm^{-2}·s^{-1}, calculated to trigger ~22 Rho* s^{-1} based on the effective collecting area of mouse rods (3). This steady background light did not significantly change flash response kinetics (Fig. 4 *A*, *Inset*). Furthermore, from the Weber–Fechner behavior of background light adaptation (Fig. 4*B*, solid curve and legend, with a background intensity that reduces flash sensitivity by half, I_o, of ~24 Rho* s^{-1}) (see also refs. 39, 46), it could be seen that even if every WT-Rho molecule in a $Rho^{WT/WT}$ rod were replaced by D190N-Rho, giving 0.008 isomerizations·s^{-1}·$cell^{-1}$ × 16 = 0.13 isomerizations·s^{-1}·$cell^{-1}$, the flash sensitivity of mouse rods would hardly change (red dashed line, Fig. 4*B*). Indeed, in order for a rhodopsin mutant to desensitize mouse rods by a factor of 2 in darkness, its spontaneous pigment-isomerization rate would need to be ~3,000-fold ($=I_o$/0.008 Rho* s^{-1}) higher than that of WT-Rho.

D190N-Rho Causes Retinal Degeneration through a Transducin-Independent Mechanism. Given the normal cellular dark noise in $Rho^{D190N/WT}$ rods, we asked whether some other aberrant side effect of phototransduction by D190N-Rho via transducin would possibly lead to degeneration (47). We bred $Rho^{D190N/D190N}$ and $Rho^{D190N/WT}$ animals into the rod transducin-α–knockout ($Gnat1^{-/-}$; ref. 48). There was severe degeneration in $Rho^{D190N/D190N}$; $Gnat1^{-/-}$ rods, with no sign of improvement over $Rho^{D190N/D190N}$; $Gnat1^{+/+}$ rods at either postnatal day 12 (P12) or P18 (Fig. 5*A*). Broadly, the same was true for $Rho^{D190N/WT}$ rods at P18, except for a slight improvement (not statistically significant) in the outer-segment length with transducin being absent (Fig. 5 *B*, *Upper Left*, verified by morphometric measurements in Fig. 5 *B*, *Upper Right*). At P100, some loss of photoreceptor nuclei in $Rho^{D190N/WT}$ was quite obvious, with also no improvement in the $Gnat1^{-/-}$ background except again for a slightly longer (statistically insignificant) outer-segment length (Fig. 5 *B*, *Lower Right*). In summary, D190N-Rho signaling via transducin appears to be unrelated to rod degeneration.

Misfolding of D190N-Rho Induces Cellular Stress. Having ruled out D190N-Rho noise as the cause of degeneration, we investigated the possible involvement of this protein's misfolding. $Rho^{D190N/D190N}$ animals had very rapid photoreceptor cell death, with obvious

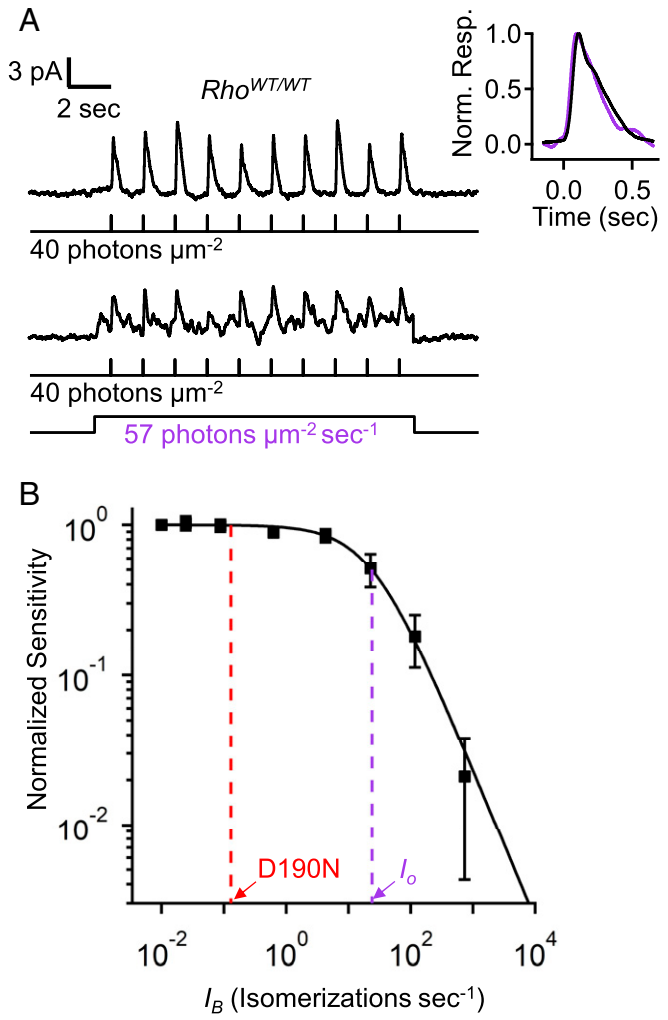

Fig. 4. Magnitude of equivalent background light for producing mouse rod desensitization. (*A*) Flash-on-background experiment with $Rho^{WT/WT}$;$Gcaps^{+/+}$ rods showing flash responses in the absence (*Top*) and presence (*Bottom*) of steady background light that reduced sensitivity approximately by half. (*Inset*) Normalized and averaged flash-response waveforms in the absence (black) or presence (purple) of the background light. (*B*) Weber–Fechner relation [$S_F/S_D = 1/(1 + I_B/I_o)$] fit to flash sensitivity (S_F) normalized to dark-adapted sensitivity (S_F/S_D) plotted against background light [I_B, converted to isomerizations·s^{-1} by multiplying with the effective collective area of mouse rods, ~0.4 μm^2 (3)]. The intensity required to reduce sensitivity by half (I_o, purple dashed line) was 63 photons·μm^{-2}·s^{-1} (~24 isomerizations·s^{-1}). If D190N-Rho content in a mouse rod was as high as endogenous WT-Rho in WT rods, the "equivalent" steady light from spontaneous D190N-Rho isomerizations would be ~0.13 isomerizations·s^{-1} (red dashed line), which would reduce a rod's sensitivity by only ~0.5%.

degeneration already at eye opening (P12). By P21, only two rows of photoreceptor nuclei remained (19). This is even more severe than the reported degeneration in homozygous rhodopsin knockout mice ($Rho^{-/-}$), in which most $Rho^{-/-}$ rod cell bodies survive until at least P30 (9). Such rapid degeneration suggests that D190N-Rho in some way exacerbates degeneration beyond simply a loss of structural support from diminished pigment content (see Introduction).

The diminution of pigment content in the outer segment in the presence of D190N-Rho suggests misfolding of a fraction of D190N-Rho molecules in the rod. Accordingly, we looked for signs of the unfolded protein response, which could cause cell death eventually through stress on the endoplasmic reticulum (21, 22, 49). Immunoblots for ATF-4 and ATF-3 [components of the PERK pathway of the unfolded protein response (22, 49)] showed a modest but significant up-regulation in retinal extracts from P18 $Rho^{D190N/WT}$ animals (Fig. 6 *A* and *B*). We also tested a dye that becomes fluorescent when trapped by misfolded-protein aggregates [PROTEOSTAT (50–52)] and found it to label more rod cell bodies in the outer nuclear layer of 1- to 2-mo $Rho^{D190N/WT}$ retinae than of $Rho^{WT/WT}$ controls (Fig. 6*C*). In some sections, this dye showed a weak background signal in the outer-segment and/or inner-segment layers as well as the outer plexiform layer, but the strongest and most consistent labeling was in some rod cell bodies. As a positive control (Fig. 6*C*), we did similar dye-labeling experiments on a mutant-rhodopsin knockin line, $Rho^{P23H/WT}$ (21), well known to show cell death through protein misfolding of P23H-Rho (53). Across all images, the average percentage of PROTEOSTAT-positive cells in each $Rho^{WT/WT}$ image was 0.03 ± 0.09% (Fig. 6*D*; $n = 24$ images) or a cell density in each animal of 0.22 ± 0.19 PROTEOSTAT-positive cells per 1,000 outer nuclear layer cells (Fig. 6*E*; $n = 3$ animals). In $Rho^{D190N/WT}$ retinal sections, the proportion of PROTEOSTAT-positive cells in each image and total cell densities in each animal were more than 10-fold higher than in $Rho^{WT/WT}$ controls, being 0.39 ± 0.29% ($n = 29$ images) and 3.86 ± 1.36 PROTEOSTAT-positive cells per 1,000 cells ($n = 3$ animals). In comparison, $Rho^{P23H/WT}$ retinal sections had 0.59 ± 0.63% labeled ONL cell bodies per image ($n = 32$ images) and 4.87 ± 0.49 PROTEOSTAT-positive cells per 1,000 outer nuclear layer cells ($n = 3$ animals). While PROTEOSTAT-positive cells were not abundant in $Rho^{D190N/WT}$ or even $Rho^{P23H/WT}$ animals, such sparse labeling has been reported for apoptotic cells in other mouse models of retinal degeneration (54).

Mechanism of D190N-Rho's Elevated Spontaneous Activity. Independent of D190N-Rho's pathogenic mechanism, we were also interested in what underlies its heightened spontaneous activity. We previously developed a physicochemical theory that predicts quite well the measured spontaneous isomerization rates across WT rod and cone pigments of multiple animal species (7, 40). In this theory, two factors govern the molecular rate constant. The first is a pigment's "critical wavelength," λ_c, which is the photon wavelength shorter than which photoexcitation of the pigment becomes temperature insensitive, thus quantifying its ground-state isomerization energy barrier, E_a, according to $E_a = hc/\lambda_c$, with h being Planck's constant and c the speed of light (7). We have found that the ratio λ_c/λ_{max}, where λ_{max} is the wavelength of maximum light absorption by the pigment, appears to be a fundamental constant equal to 0.84 ± 0.01 [$n = 7$ pigments (7)], although no disease-inducing mutant pigments have yet been tested up to now.

The second factor has to do with physical constraints in the pigment's chromophore-binding pocket, which, in our theory, manifests as a proportionality constant equivalent to the "pre-exponential factor" in reaction rate theory in physical chemistry (7). Past measurements by us from several native rod and cone pigments have indicated that this proportionality constant is empirically ~26 times higher for native cone pigments than for native rod pigments (7). Cone pigments are known to have a more accessible chromophore-binding pocket, exhibiting the property of spontaneous chromophore exchange in darkness not found in rod pigments (40, 55, 56). Accordingly, we have hypothesized a correlation between this dark-chromophore exchange property and a steric openness (i.e., less restrictiveness for molecular motion of the chromophore) of the binding pocket, hence giving a larger proportionality constant for spontaneous isomerization (7, 40). This correlation is only qualitative, however, in that a ~26-fold difference in the multiplication factor does not have to be constant between all rod pigments and all cone pigments. After all, gradations in the openness of the chromophore binding pocket can in principle exist.

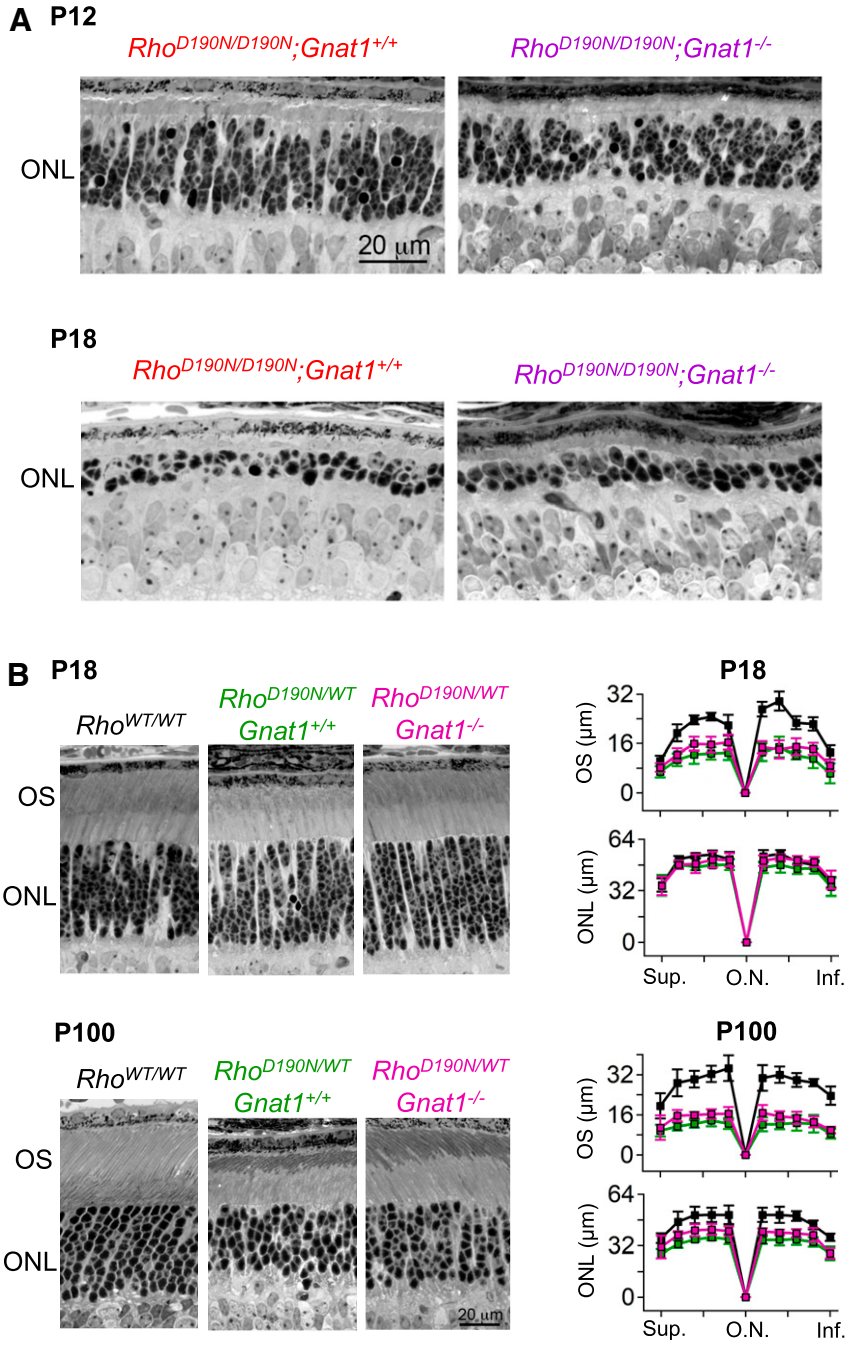

Fig. 5. D190N-Rho causes retinal degeneration by a transducin-independent mechanism. (*A*, *Top Left*) Representative retinal cross-section from a $Rho^{D190N/D190N}$ animal at eye opening, P12. The outer nuclear layer (ONL) was thinner than in P12 $Rho^{WT/WT}$ (see ref. 19). (*A*, *Top Right*) Cross-section from a $Rho^{D190N/D190N}$;$Gnat1^{-/-}$ animal at eye opening, P12. (*A*, *Bottom Left*) Representative retinal cross-section from a $Rho^{D190N/D190N}$ animal at P18, when rod outer segments are fully mature in $Rho^{WT/WT}$ rods. Severe degeneration led to only two to three rods remaining in each ONL column. (*A*, *Bottom Right*) The ONL thickness was similar in $Rho^{D190N/D190N}$;$Gnat1^{-/-}$ demonstrating that the $Gnat1^{-/-}$ background did not prevent degeneration. (*B*, *Top Left*) Histological sections at P18 from $Rho^{WT/WT}$, $Rho^{D190N/WT}$;$Gnat1^{+/+}$ and $Rho^{D190N/WT}$;$Gnat1^{-/-}$. (*B*, *Top Right*) Outer nuclear layer thickness (ONL) and approximate outer segment length (OS) quantified along the superior–inferior axis along the central meridian ($n = 4$ to 9 animals; mean ± SD). (*B*, *Bottom*) Histological sections from P100 animals and the corresponding morphometric analysis. One-way ANOVA was calculated to detect differences in ONL thickness and OS length between the three groups, followed by Tukey HSD. $Rho^{D190N/WT}$;$Gnat1^{+/+}$ and $Rho^{D190N/WT}$;$Gnat1^{-/-}$ groups showed no difference at all retinal regions in P18 and P100 sections, whereas both were significantly different from $Rho^{WT/WT}$ retinae in P18 OS length and in P100 ONL thickness and OS length ($0.0001 \leq P \leq 0.05$). Inf., inferior; O.N., optic nerve; Sup., superior.

With the above background, the relevant factors determining the thermal isomerization of D190N-Rho in $Rho^{D190N/REY}$ can now be presented. By using dim-flash responses to measure rod spectral sensitivity at 37 and 25 °C, we found that the λ_c/λ_{max} ratio for D190N-Rho in $Rho^{D190N/REY}$ rods (Fig. 7) indeed adheres to the universal constant of 0.84 ± 0.01 (7). We confirmed this parameter to be ∼0.83 for WT-Rho in $Rho^{WT/WT}$ rods (Fig. 7*A*), and the same for D190N-Rho in $Rho^{D190N/REY}$ rods (Fig. 7*B*), thus giving, together with a λ_{max} of ∼500 nm for both WT-Rho and D190N-Rho, an isomerization energy barrier (E_a) of ∼47 kcal·mol^{-1}.

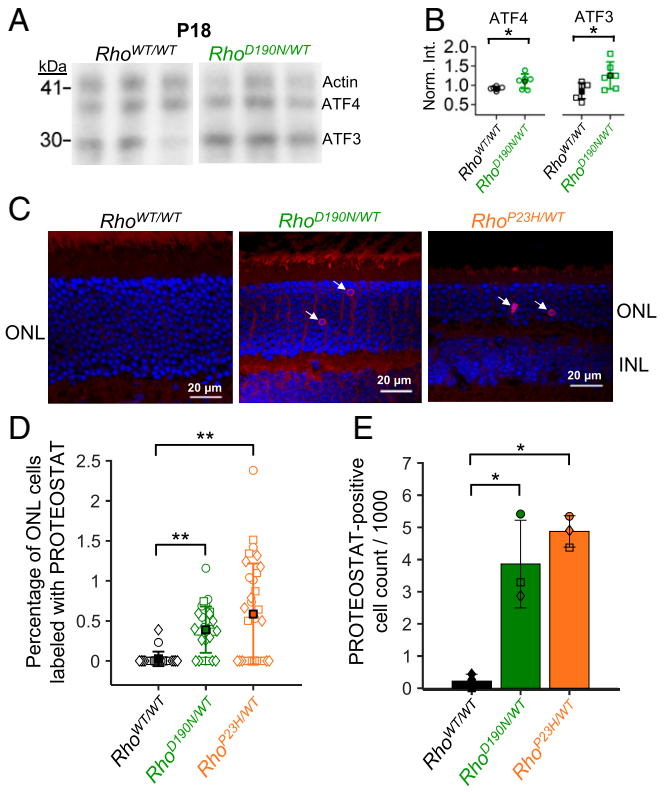

Fig. 6. Induction of the unfolded protein response and detection of misfolded protein aggregates. (*A*) Immunoblots of ATF4 and ATF3, which are involved in the unfolded protein response. Actin was costained for normalization. Blots from three animals each of P18 $Rho^{WT/WT}$ (*Left*) and $Rho^{D190N/WT}$ (*Right*) are shown. (*B*) Band intensity normalized to actin for each sample. Both ATF4 and ATF3 were significantly up-regulated in retinal extracts from P18 $Rho^{D190N/WT}$;$Gnat1^{+/+}$ animals ($P < 0.05$). (*C*) Cryosections and fluorescent labeling using PROTEOSTAT dye to stain $Rho^{WT/WT}$ (*Left*), $Rho^{D190N/WT}$ (*Middle*), and $Rho^{P23H/WT}$ (*Right*) retinae. (*D*) Percentage of PROTEOSTAT-positive cells across images. Each symbol represents the percentage from a single image as shown in *C*. Circles, squares, and diamonds represent data from each of three animals. (*E*) Overall density of PROTEOSTAT-positive cells per 1,000 cell bodies counted in the outer nuclear layer in each animal ($n = 3$ animals). Each symbol (circle, square, or diamond) represents the PROTEOSTAT-positive cell density from an individual animal. The single stars mark statistical significance of $0.0001 \leq P \leq 0.05$, and the double stars mark $P < 0.0001$. Comparing $Rho^{D190N/WT}$ and $Rho^{P23H/WT}$, there was not a statistically significant difference in the densities of PROTEOSTAT-positive cells.

Next, we checked the property of chromophore exchange in darkness in D190N-Rho. The molecular rate of chromophore exchange in WT-Rho is exceedingly low, being reported to be on average only once every 52 d at 37 °C (57), versus only hours at room temperature (40) for the relatively more "open" binding pocket of cone pigments. We heterologously expressed D190N-Rho in HEK293 cells and extracted the protein for in vitro spectroscopic measurements (*SI Appendix*, *Supplementary Methods*). We then tracked any exchange of native 11-*cis*-retinal with exogenous 9-*cis*-retinal in darkness as indicated by a gradual blueshift in λ_{max} (40, 55, 56). We found that mouse D190N-Rho could not be reconstituted in vitro, perhaps due to some misfolding/mistargeting even at room temperature (*SI Appendix*, Fig. S3*A*), similar to what has been reported for human D190N-Rho in HEK293 cells (26). In contrast, bovine D190N-Rho could be reconstituted and incubated at 37 °C for up to 20 d, albeit with steady thermal deterioration (*SI Appendix*, Fig. S3 *B* and *C*).

For chromophore exchange, parallel experiments were done on bovine WT-Rho, bovine D190N-Rho, and chicken M-cone pigment for comparison. Chicken M-cone pigment was used because of its lower rate of deterioration in vitro than for the mouse homolog. Dark-state bovine WT-Rho had a λ_{max} of 503.5 nm (Fig. 8 *A*, *Left*) and shifted only slightly (by −5.2 nm) after a 10-d incubation at 37 °C with 9-*cis*-retinal to 498.3 ± 0.6 nm (Fig. 8 *B*, *Left*; $n = 3$). Dark-state bovine D190N-Rho's λ_{max} was 502.8 nm (Fig. 8 *A*, *Center*) and shifted only ever so slightly (by −3.3 nm) to 499.5 ± 1.8 nm (Fig. 8 *B*, *Center*; $n = 3$) after the same 9-*cis*-retinal treatment for 10 d. Contrastingly, chicken M-cone pigment showed a much faster and more obvious chromophore exchange, with its dark-state λ_{max} of 510.5 nm (Fig. 8 *A*, *Right*) shifting (by −12.1 nm) after only 30 h at 20 °C to 498.4 ± 0.7 nm (Fig. 8 *B*, *Right*; $n = 3$). To demonstrate the maximal shifts, we fully reconstituted each pigment with 9-*cis*-retinal (Fig. 8*C*), which gave λ_{max} shifts of −14.0, −13.3, and −20.5 nm for WT-Rho, D190N-Rho, and M-cone pigment, respectively. While these measurements

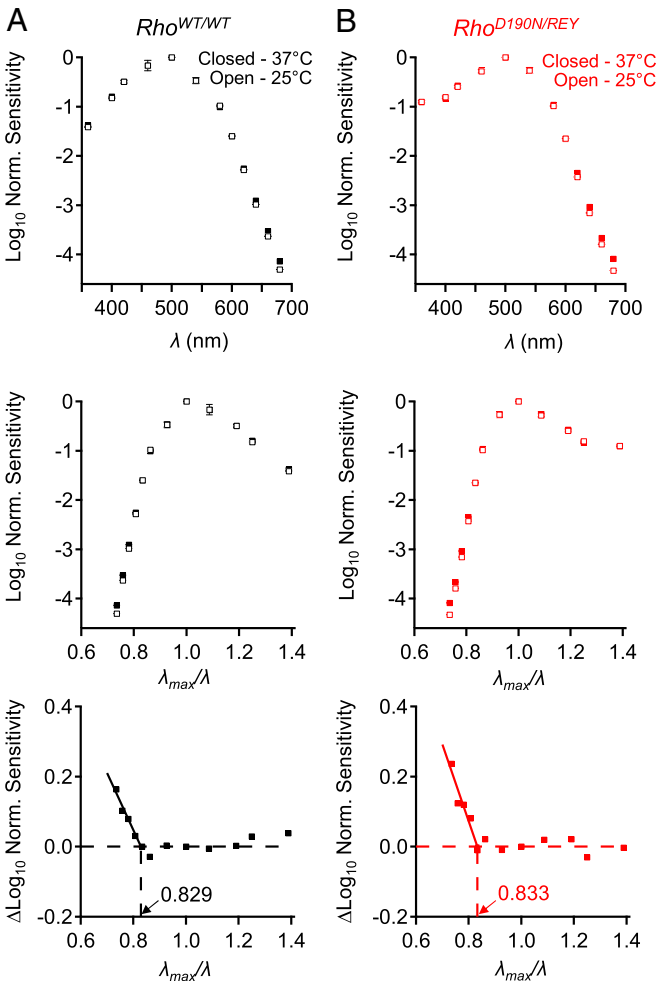

Fig. 7. The isomerization energy barrier is unchanged in D190N-Rho. (*A*, *Top*) Control experiments with $Rho^{WT/WT}$ (C57BL/6J) rods showing the effect of temperature on normalized action spectra at 25 °C (open symbols) and at 37 °C (closed symbols). (*A*, *Middle*) Plotting normalized sensitivity on a reciprocal-wavelength plot with λ_{max}/λ as the abscissa. (*A*, *Bottom*) Subtraction of the 25 °C spectrum from the 37 °C spectrum shows enhancement of photosensitivity by heat at longer wavelengths (i.e., lower-energy photons). (*B*) Corresponding experiments with $Rho^{D190N/REY}$ rods. Peak sensitivity was at ~500 nm for both WT-Rho and D190N-Rho. For $Rho^{WT/WT}$ rods, temperature enhancement began at $\lambda_{max}/\lambda = 0.829$ corresponding to an isomerization energy barrier of ~47.4 kcal·mol^{-1} in WT-Rho, and for $Rho^{D190N/REY}$ rods, $\lambda_{max}/\lambda = 0.833$ indicating an isomerization energy barrier of ~47.7 kcal·mol^{-1} in D190N-Rho.

were largely qualitative, D190N-Rho's exceedingly slow chromophore exchange behavior clearly resembled that of WT-Rho.

From the above experiments, it seems that the much higher spontaneous activity of D190N-Rho measured physiologically in live rods could not be explained by a shallowing of its isomerization energy barrier or from an open chromophore-binding pocket resembling that in cone pigments. On the other hand, a mutation such as D190N, which is situated directly above the chromophore-binding pocket, could conceivably still give more freedom of movement to the chromophore (hence a larger preexponential factor, albeit <26-fold) without necessarily opening the binding pocket enough to increase chromophore exchange as that shown by cone pigments. It is not yet known exactly how the "openness" of the chromophore-binding pocket and the preexponential factor from our pigment noise theory (7) are influenced by the bond energies in the hydrogen-bond network formed between D190 and neighboring residues within the chromophore-binding pocket (16, 31).

Discussion

Some rhodopsin mutations causing night blindness followed by retinal degeneration have been speculated to do so by producing a higher frequency of spontaneous isomerization events (reviewed in ref. 45). Spontaneous-isomerization noise is particularly amenable to physiological study (6, 7, 39, 40, 58), prompting us to examine this property regarding D190N-Rho. By silencing the endogenous rhodopsin signal sufficiently through replacing it with the mutant rhodopsin, REY-Rho, we were able to quantify D190N-Rho's dark noise in mouse rods. We found that D190N-Rho indeed had over an order-of-magnitude higher molecular rate constant of spontaneous isomerization compared to WT-Rho. Nonetheless, because of the diminished D190N-Rho content in $Rho^{D190N/REY}$ and $Rho^{D190N/WT}$ animals, this elevation in molecular noise actually does not increase the overall cellular dark noise. Thus, the higher molecular D190N-Rho spontaneous activation compared to WT-Rho does not cause rod desensitization or, more importantly, underlie degeneration of $Rho^{D190N/WT}$ mouse rods. The lack of improvement of the condition in a transducin-knockout background further supported this conclusion. Assuming that the data from the genetic mouse model are valid for human patients, this rather surprising conclusion importantly demonstrates that in vitro measurements, albeit important for capturing certain salient protein properties, can still miss key subtleties that are evident only in live rods.

It would be interesting to know whether our understanding gained here applies to some other disease-causing rhodopsin mutants also thought to have higher spontaneous activity. In this regard, another extensively studied disease-causing rhodopsin mutation, G90D-Rho, has been found to destabilize a crucial ionic bond (E113 to K296) normally preventing dark-state WT-Rho from signaling (59), thus constitutively triggering activation of transducin by exposing the G-protein interaction site without canonical isomerization of 11-*cis*-retinal (30, 59, 60). Curiously, dark electrical noise did not appear substantially elevated in transgenic mouse rods expressing G90D-Rho despite signs of adaptation to an equivalent background light estimated to be ~130 Rho* s^{-1}·$cell^{-1}$ (13, 14). Other disease-causing mutations, such as T94I-, A292E-, and A295V-Rho, have also been speculated to show dark-state constitutive activity without canonical chromophore isomerization (30, 45, 61), but these mutations lack animal models for in vivo confirmation. Mechanistic uncertainties likewise remain for G90V, E113Q, S186W, and K296G (16, 30, 45). As illustrated by G90D-Rho, constitutive pigment activity measured biochemically does not necessarily translate into a measurable elevation in dark electrical noise in intact photoreceptors. As a separate example, K296E-Rho lacks the chromophore linkage site and results in heightened constitutive apo-opsin activity in vitro (28). This mutation causes rod degeneration in vivo—not due to elevated dark noise—but primarily from rhodopsin being retained in the inner segment bound to arrestin, which induces cell stress because of the inability of apo-opsin to convert to dark-state rhodopsin (23, 24).

In the particularly debatable case of D190N-Rho (16, 19, 26, 27, 31, 35), our results suggest that the main phenotype is a reduction in the functional pigment content due to protein misfolding, resulting in a shortened outer-segment length and a faster response shutoff rather similar to heterozygous rhodopsin-knockout rods (9–11, 38). Similarly, isoelectric focusing experiments showed that D190N-Rho comprised approximately only one-third of the visual pigment in both $Rho^{D190N/REY}$ and $Rho^{D190N/WT}$ retinae. Of note, nonetheless, is that those D190N-Rho molecules that traffic successfully to the outer segment respond to light literally identically to WT-Rho, based on suction pipette recordings from $Rho^{D190N/REY}$ rods, Previous studies of $Rho^{D190N/WT}$ animals were unable to detect mistargeted D190N-Rho by immunostaining or immunoblots with anti-Rho antibodies (19, 32), perhaps due to rapid degradation of misfolded D190N-Rho. Such degradation could help explain why many $Rho^{D190N/WT}$ rods are able to tolerate the presence of D190N-Rho for months in mice (and decades in human patients) before the mutant pigment triggers rod death.

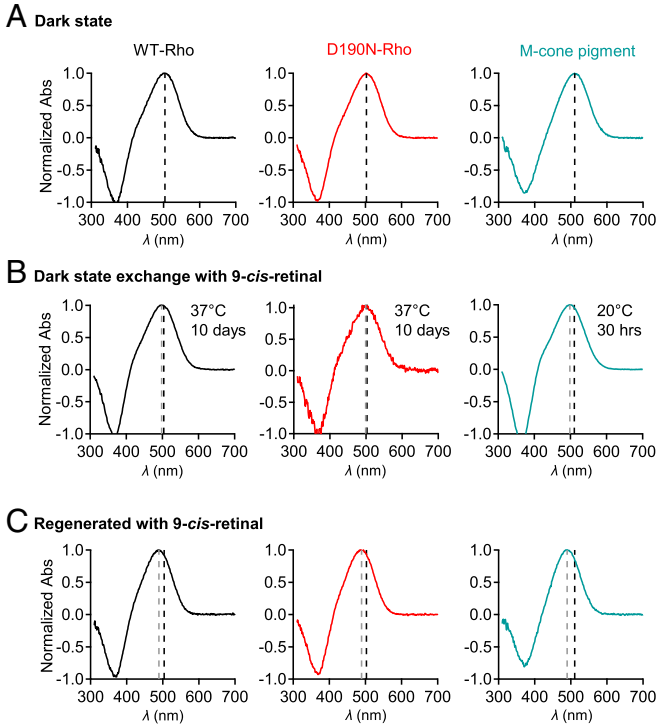

Fig. 8. Chromophore exchange in D190N-Rho. (*A*) Dark absorption spectra (normalized against peak optical density) of bovine WT-Rho (black), bovine D190N-Rho (red), and chicken M-cone pigment (teal), bound to 11-*cis*-retinal. The black dashed lines are λ_{max} values for each pigment (503.8, 502.5, and 510.5 nm, respectively). (*B*) Chromophore exchange experiment involving exposure of bovine WT-Rho and D190N-Rho (for 10 d at 37 °C) or of chicken M-cone pigment (for 30 h at 20 °C) to 9-*cis*-retinal. The gray dashed lines are blue-shifted λ_{max} after exchange of 9-*cis*-retinal for 11-*cis*-retinal after the labeled exposure times. The λ_{max} shifts were −5.5 ± 0.6 nm (n = 3 preparations) for WT-Rho, −3.3 ± 1.8 nm (n = 3 preparations) for D190N-Rho, and −12.1 ± 0.7 nm (n = 3 preparations) for M-cone pigment. There was no significant difference between the λ_{max}-shift values of D190N-Rho and WT-Rho (P = 0.16). (*C*) Maximally blue-shifted spectra from full regeneration with 9-*cis*-retinal, starting with respective opsin, giving λ_{max} shifts to 489.5 nm (WT-Rho), 489 nm (D190N-Rho), and 490 nm (chicken M-cone pigment).

We found a modest induction of the unfolded protein response as well as occasional rods showing misfolded-protein aggregates accompanying the gradual degeneration in $Rho^{D190N/WT}$ retinae. In contrast, homozygous $Rho^{D190N/D190N}$ rods do not form an outer segment at all and the rate of retinal degeneration is even more rapid than $Rho^{-/-}$ rods (9, 19). Thus, possibly, the trafficking and/or stability of D190N-Rho is contingent on the presence of WT-Rho. On the other hand, the presence of D190N-Rho appears to impact negatively the overall Rho content in $Rho^{D190N/WT}$ rods. An important remaining question is what can be done to prevent vision loss. Our findings demonstrate that D190N-Rho does not desensitize rods through elevated spontaneous activity; instead, the mutation leads to disruption of rhodopsin's structural support of the outer segment, loss of photon capture, and mild induction of the unfolded protein response. Gene therapy using CRISPR/Cas9 to correct the D190N mutation has been proposed as one possible solution (62), but it is important to keep in mind that early intervention might be required for maintaining healthy rod morphology.

Methods

Analyses of Flash Responses and Dark Noise. Suction pipette recording was used to record flash responses and dark noise (*SI Appendix*, *Supplementary Methods*), 10 to 30 flash responses were measured at each flash strength (with fewer flashes for saturated responses). Transient peaks of mean responses were used to determine the intensity–response relation for each cell by fitting to a saturating-exponential function $R/R_{max} = 1 - \exp(-I_F \times K)$, where R is response peak, R_{max} is saturated-response peak, I_F is flash strength (in photons per square micrometer), and K is a constant. The half-saturating flash strength, ρ, is given by $\rho = \log_e(2)/K$. To evaluate single-photon responses, we measured 30 to 100 dim-flash responses at an intensity within the linear foot of the intensity–response relation. Quantal analyses and determination of flash response parameters (integration time, time-to-peak, and recovery time constant) were carried out as described previously (3).

To measure thermal isomerization events in mouse rods, we needed extremely stable recording and low instrumental noise. Recordings were optimized using pipettes with a tip opening of ~1.5 to 1 μm and a resistance of ~7 to 8 MΩ in recording solutions at room temperature. To minimize the slow electronic drift, we used a custom-made chamber with an exit port lined with a piece of absorbent tissue paper (Kimberly-Clark Professional; Kimtech Science, Kimwipe) that would wick away solution at the same speed that it entered the chamber. The ground electrode holder (World Precision Instruments; MEH3S10) was filled with pipette solution and connected to the bath by a glass capillary filled with 1 M KCl in 3% agar gel. Dark noise was recorded in 10-min epochs. Discrete events were counted using custom MATLAB (MathWorks) software with the criteria of peak amplitude >30% of the single-photon response peak and duration of 50 to 200% of the integration time of the single-photon response measured from the same cell.

Estimating Rho Content from the Probability of Failure. According to the Poisson distribution of photon absorption (42), the probability of failure (p_0) is given by $p_0 = \exp(-A_C \times I_F)$, where A_C is the effective collecting area of an outer segment (in square micrometers) and I_F is flash strength (in photons per square micrometer). A failure was defined as a flash trial that did not result in a response reaching a criterion amplitude (typically ≥50% of the single-photon response peak) within a characteristic time window based on the average response waveform. The computed probability of failure was routinely verified by inspecting each flash response trial. A_C is a function of effective-Rho content in the outer segment and Rho's light absorption properties (3, 42), $A_C = V \times \delta \times \alpha_\lambda \times f \times Q$, where V is the volume of outer segment, δ is the concentration of functional Rho molecules in the outer segment (the unknown parameter, with units of molecules per cubic micrometer), α_λ is the molecular extinction coefficient of Rho (63) oriented in an outer segment disk membrane [$\sim 1.76 \times 10^{-8}$ μm^2 for WT-Rho based on microspectrophotometry (2, 3), with this parameter being 6% lower for D190N-Rho (16)], Q is the probability that an absorbed photon leads to isomerization [0.67 (63)], and f is a polarization factor due to the orientation of rhodopsin approximately perpendicular to the outer segment long axis [0.5 for transverse illumination with unpolarized light (42)]. Thus, the probability of failure can be used to estimate the number of effective Rho molecules (n) in a rod as follows:

$$A_C = \log_e(p_0)/(-I_F), \quad [1]$$

$$\delta = A_C/[V \times \alpha_\lambda \times f \times Q], \quad [2]$$

$$n = \delta \times V. \quad [3]$$

Data Availability. All study data are included in the article and *SI Appendix*.

ACKNOWLEDGMENTS. We thank Drs. Chyuan-Sheng Lin (Columbia University) and Janis Lem (Tufts University) for generating the $Rho^{D190N/D190N}$ and $Gnat1^{-/-}$ mouse lines, respectively. We also thank Dr. Jeremy Nathans, Dr. Jacob S. Heng, and members of the K.-W.Y. laboratory for discussions. This work was supported by NIH Grants EY006837 (to K.-W.Y.); EY012155 and EY027193 (to J.C.); Vision Core Grant P30EY029220 (to the Roski Eye Institute at University of Southern California); EY018213 and EY024698; and the Crowley Family Fund (to S.H.T.); CREST, Japan Science and Technology Agency Grant JPMJCR1753 (to T.Y.); the António Champalimaud Vision Award, Portugal (to K.-W.Y.); NIH Grant NS050274 (Multiphoton Imaging Core at Johns Hopkins University); and the Visual Science Training Program Fellowship from the National Eye Institute, Grant EY007143 (to D.S.).

1. S. Hecht, S. Shlaer, M. H. Pirenne, Energy, quanta and vision. *J. Gen. Physiol.* **25**, 819–840 (1942).
2. F. I. Hárosi, Absorption spectra and linear dichroism of some amphibian photoreceptors. *J. Gen. Physiol.* **66**, 357–382 (1975).
3. W. W. S. Yue *et al*., Elementary response triggered by transducin in retinal rods. *Proc. Natl. Acad. Sci. U.S.A.* **116**, 5144–5153 (2019).
4. I. B. B. Leskov *et al*., The gain of rod phototransduction: Reconciliation of biochemical and electrophysiological measurements. *Neuron* **27**, 525–537 (2000).
5. V. Y. Arshavsky, M. E. Burns, Current understanding of signal amplification in phototransduction. *Cell. Logist.* **4**, e29390 (2014).
6. D. A. Baylor, G. Matthews, K. W. Yau, Two components of electrical dark noise in toad retinal rod outer segments. *J. Physiol.* **309**, 591–621 (1980).
7. D.-G. Luo, W. W. S. Yue, P. Ala-Laurila, K.-W. Yau, Activation of visual pigments by light and heat. *Science* **332**, 1307–1312 (2011).
8. M. M. Humphries *et al*., Retinopathy induced in mice by targeted disruption of the rhodopsin gene. *Nat. Genet.* **15**, 216–219 (1997).
9. J. Lem *et al*., Morphological, physiological, and biochemical changes in rhodopsin knockout mice. *Proc. Natl. Acad. Sci. U.S.A.* **96**, 736–741 (1999).
10. C. L. Makino *et al*., Rhodopsin expression level affects rod outer segment morphology and photoresponse kinetics. *PLoS One* **7**, e37832 (2012).
11. Y. Liang *et al*., Rhodopsin signaling and organization in heterozygote rhodopsin knockout mice. *J. Biol. Chem.* **279**, 48189–48196 (2004).
12. J. Nathans, In the eye of the beholder: Visual pigments and inherited variation in human vision. *Cell* **78**, 357–360 (1994).
13. P. A. Sieving *et al*., Constitutive "light" adaptation in rods from G90D rhodopsin: A mechanism for human congenital nightblindness without rod cell loss. *J. Neurosci.* **21**, 5449–5460 (2001).
14. A. M. Dizhoor *et al*., Night blindness and the mechanism of constitutive signaling of mutant G90D rhodopsin. *J. Neurosci.* **28**, 11662–11672 (2008).
15. S. Jin, M. C. Cornwall, D. D. Oprian, Opsin activation as a cause of congenital night blindness. *Nat. Neurosci.* **6**, 731–735 (2003).
16. M. Y. Liu *et al*., Thermal stability of rhodopsin and progression of retinitis pigmentosa: Comparison of S186W and D190N rhodopsin mutants. *J. Biol. Chem.* **288**, 17698–17712 (2013).
17. C. Zeitz *et al*., Identification and functional characterization of a novel rhodopsin mutation associated with autosomal dominant CSNB. *Invest. Ophthalmol. Vis. Sci.* **49**, 4105–4114 (2008).
18. T. P. Dryja, E. L. Berson, V. R. Rao, D. D. Oprian, Heterozygous missense mutation in the rhodopsin gene as a cause of congenital stationary night blindness. *Nat. Genet.* **4**, 280–283 (1993).
19. J. Sancho-Pelluz *et al*., Mechanisms of neurodegeneration in a preclinical autosomal dominant retinitis pigmentosa knock-in model with a Rho^{D190N} mutation. *Cell. Mol. Life Sci.* **76**, 3657–3665 (2019).
20. R. R. Franke, B. König, T. P. Sakmar, H. G. Khorana, K. P. Hofmann, Rhodopsin mutants that bind but fail to activate transducin. *Science* **250**, 123–125 (1990).
21. S. Sakami *et al*., Probing mechanisms of photoreceptor degeneration in a new mouse model of the common form of autosomal dominant retinitis pigmentosa due to P23H opsin mutations. *J. Biol. Chem.* **286**, 10551–10567 (2011).
22. D. Athanasiou *et al*., The role of the ER stress-response protein PERK in rhodopsin retinitis pigmentosa. *Hum. Mol. Genet.* **26**, 4896–4905 (2017).
23. J. Chen *et al*., Stable rhodopsin/arrestin complex leads to retinal degeneration in a transgenic mouse model of autosomal dominant retinitis pigmentosa. *J. Neurosci.* **26**, 11929–11937 (2006).
24. H. Moaven *et al*., Visual arrestin interaction with clathrin adaptor AP-2 regulates photoreceptor survival in the vertebrate retina. *Proc. Natl. Acad. Sci. U.S.A.* **110**, 9463–9468 (2013).
25. C. H. Sung *et al*., Rhodopsin mutations in autosomal dominant retinitis pigmentosa. *Proc. Natl. Acad. Sci. U.S.A.* **88**, 6481–6485 (1991).

26. C. H. Sung, C. M. Davenport, J. Nathans, Rhodopsin mutations responsible for autosomal dominant retinitis pigmentosa. Clustering of functional classes along the polypeptide chain. *J. Biol. Chem.* **268**, 26645–26649 (1993).
27. S. Kaushal, H. G. Khorana, Structure and function in rhodopsin. 7. Point mutations associated with autosomal dominant retinitis pigmentosa. *Biochemistry* **33**, 6121–6128 (1994).
28. P. R. Robinson, G. B. Cohen, E. A. Zhukovsky, D. D. Oprian, Constitutively active mutants of rhodopsin. *Neuron* **9**, 719–725 (1992).
29. V. R. Rao, G. B. Cohen, D. D. Oprian, Rhodopsin mutation G90D and a molecular mechanism for congenital night blindness. *Nature* **367**, 639–642 (1994).
30. V. R. Rao, D. D. Oprian, Activating mutations of rhodopsin and other G protein-coupled receptors. *Annu. Rev. Biophys. Biomol. Struct.* **25**, 287–314 (1996).
31. J. M. Janz, J. F. Fay, D. L. Farrens, Stability of dark state rhodopsin is mediated by a conserved ion pair in intradiscal loop E-2. *J. Biol. Chem.* **278**, 16982–16991 (2003).
32. J. Sancho-Pelluz *et al*., Mice with a D190N mutation in the gene encoding rhodopsin: A model for human autosomal-dominant retinitis pigmentosa. *Mol. Med.* **18**, 549–555 (2012).
33. I. Tsui, C. L. Chou, N. Palmer, C. S. Lin, S. H. Tsang, Phenotype-genotype correlations in autosomal dominant retinitis pigmentosa caused by RHO, D190N. *Curr. Eye Res.* **33**, 1014–1022 (2008).
34. G. A. Fishman *et al*., Ocular findings associated with rhodopsin gene codon 267 and codon 190 mutations in dominant retinitis pigmentosa. *Arch. Ophthalmol.* **110**, 1582–1588 (1992).
35. J. M. Janz, D. L. Farrens, Assessing structural elements that influence Schiff base stability: Mutants E113Q and D190N destabilize rhodopsin through different mechanisms. *Vision Res.* **43**, 2991–3002 (2003).
36. K. Nakatani, K.-W. Yau, Calcium and light adaptation in retinal rods and cones. *Nature* **334**, 69–71 (1988).
37. G. L. Fain, H. R. Matthews, M. C. Cornwall, Y. Koutalos, Adaptation in vertebrate photoreceptors. *Physiol. Rev.* **81**, 117–151 (2001).
38. P. D. Calvert *et al*., Membrane protein diffusion sets the speed of rod phototransduction. *Nature* **411**, 90–94 (2001).
39. Y. Fu, V. Kefalov, D.-G. Luo, T. Xue, K.-W. Yau, Quantal noise from human red cone pigment. *Nat. Neurosci.* **11**, 565–571 (2008).
40. W. W. S. Yue *et al*., Spontaneous activation of visual pigments in relation to openness/closedness of chromophore-binding pocket. *eLife* **6**, e18492 (2017).
41. M. E. Burns, A. Mendez, J. Chen, D. A. Baylor, Dynamics of cyclic GMP synthesis in retinal rods. *Neuron* **36**, 81–91 (2002).
42. D. A. Baylor, T. D. Lamb, K.-W. Yau, Responses of retinal rods to single photons. *J. Physiol.* **288**, 613–634 (1979).
43. S. Lokappa, M. Cornwall, J. Chen, Isoelectric focusing to quantify rhodopsin phosphorylation in mouse retina. *Bio Protoc.* **9**, e3300 (2019).
44. J. Berry *et al*., Effect of rhodopsin phosphorylation on dark adaptation in mouse rods. *J. Neurosci.* **36**, 6973–6987 (2016).
45. P. S.-H. Park, Constitutively active rhodopsin and retinal disease. *Adv. Pharmacol.* **70**, 1–36 (2014).
46. J. Fan, M. L. Woodruff, M. C. Cilluffo, R. K. Crouch, G. L. Fain, Opsin activation of transduction in the rods of dark-reared Rpe65 knockout mice. *J. Physiol.* **568**, 83–95 (2005).
47. A. Majumder *et al*., Transducin translocation contributes to rod survival and enhances synaptic transmission from rods to rod bipolar cells. *Proc. Natl. Acad. Sci. U.S.A.* **110**, 12468–12473 (2013).
48. P. D. Calvert *et al*., Phototransduction in transgenic mice after targeted deletion of the rod transducin alpha -subunit. *Proc. Natl. Acad. Sci. U.S.A.* **97**, 13913–13918 (2000).
49. T. Wang, J. Chen, Induction of the unfolded protein response by constitutive G-protein signaling in rod photoreceptor cells. *J. Biol. Chem.* **289**, 29310–29321 (2014).
50. D. Shen *et al*., Novel cell- and tissue-based assays for detecting misfolded and aggregated protein accumulation within aggresomes and inclusion bodies. *Cell Biochem. Biophys.* **60**, 173–185 (2011).
51. J. Ou *et al*., iPSCs from a hibernator provide a platform for studying cold adaptation and its potential medical applications. *Cell* **173**, 851–863.e16 (2018).
52. K. K. Jena *et al*., TRIM16 controls assembly and degradation of protein aggregates by modulating the p62-NRF2 axis and autophagy. *EMBO J.* **37**, e98358 (2018).
53. W. C. Chiang *et al*., Robust endoplasmic reticulum-associated degradation of rhodopsin precedes retinal degeneration. *Mol. Neurobiol.* **52**, 679–695 (2015).
54. C. Portera-Cailliau, C. H. Sung, J. Nathans, R. Adler, Apoptotic photoreceptor cell death in mouse models of retinitis pigmentosa. *Proc. Natl. Acad. Sci. U.S.A.* **91**, 974–978 (1994).
55. H. Matsumoto, F. Tokunaga, T. Yoshizawa, Accessibility of the iodopsin chromophore. *Biochim. Biophys. Acta* **404**, 300–308 (1975).
56. V. J. Kefalov *et al*., Breaking the covalent bond—a pigment property that contributes to desensitization in cones. *Neuron* **46**, 879–890 (2005).
57. H. Tian, T. P. Sakmar, T. Huber, Measurement of slow spontaneous release of 11-*cis*-retinal from rhodopsin. *Biophys. J.* **112**, 153–161 (2017).
58. V. Kefalov, Y. Fu, N. Marsh-Armstrong, K.-W. Yau, Role of visual pigment properties in rod and cone phototransduction. *Nature* **425**, 526–531 (2003).
59. A. Singhal *et al*., Insights into congenital stationary night blindness based on the structure of G90D rhodopsin. *EMBO Rep.* **14**, 520–526 (2013).
60. T. A. Zvyaga, K. Fahmy, F. Siebert, T. P. Sakmar, Characterization of the mutant visual pigment responsible for congenital night blindness: A biochemical and Fourier-transform infrared spectroscopy study. *Biochemistry* **35**, 7536–7545 (1996).
61. A. Singhal *et al*., Structural role of the T94I rhodopsin mutation in congenital stationary night blindness. *EMBO Rep.* **17**, 1431–1440 (2016).
62. Y.-T. Tsai *et al*., Clustered regularly interspaced short palindromic repeats-based genome surgery for the treatment of autosomal dominant retinitis pigmentosa. *Ophthalmology* **125**, 1421–1430 (2018).
63. H. J. A. Dartnall, "Photosensitivity" in *Handbook of Sensory Physiology*, H. J. A. Dartnall, Ed. (Springer, New York, 1972), Vol. 7, pp. 122–145.